Figure S1

Figure S1. *Il22*^{hCD4} construct design and characterization. Related to Figure 1.
(A) *Il22*^{hCD4} mice were generated using a targeting cassette containing an EMCV IRES, truncated human CD4 (hCD4) gene, and a frt-flanked (◊) neomycin resistance cassette. LoxP (O) sites were placed upstream of exon 1 and into the fifth exon of the *Il22* gene, immediately 3' of the stop codon (*) and 5' of the 3' untranslated region of exon 5. The targeting cassette was transfected into Bruce4 mouse ES cells and Ganciclovir/G418-resistant clones were screened for correct targeting of the *Il22* gene by Southern blot analysis (B) (N, non-targeted; A, *Il22* allele targeted; B, *Iltifb* allele targeted). (C) T cells from WT or *Il22*^{hCD4} mice were differentiated *in vitro* with IL-6 (10 ng/ml) and IL-23 (10 ng/ml) for 4-5 days. T cells were restimulated with PMA/Ionomycin and Brefeldin A, and then surface stained for TCRβ, mCD4, hCD4, and Live/Dead dye, followed by intracellular staining for IL-22 and analyzed by flow cytometry; mCD4$^-$ cells (red), mCD4$^+$ cells (blue). 3 mice, 2 independent experiments. (D) Colon cells from D8/9 *C.r*-infected *Il22*^{hCD4} mice were stimulated with PMA/Ion and IL-23 for 4 hrs and then stained for TCRβ, hCD4, mCD4, TCRγδ, CD45 and L/D dye and analyzed by flow cytometry. 3 mice, 2 independent experiments. (E) Cells isolated from either colon or dLN (draining lymph nodes; pooled distal mesenteric and caudal) from D8 *C.r*-infected *Il22*^{hCD4} mice were stimulated with P/I and IL-23 for 4 hrs and then sorted into TCRβ$^-$hCD4$^+$ innate cells and TCRβ$^+$hCD4$^+$ T cells. After sorting, innate cells and T cells were re-stimulated with P/I and IL-23 for 24 hrs and supernatant was collected and analyzed for IL-22 by ELISA. 2 mice, 3 independent experiments. (F-H) Naïve CD4$^+$ T cells from *Il22*$^{hCD4/null}$ (blue) or *IL22*$^{hCD4/hCD4}$ (red) mice were differentiated *in vitro* with IL-6 (40 ng/ml) and IL-23 (20 ng/ml) for 3 days, followed by PMA/Ion stimulation for 4 hrs. 1-2 mice per group, 2 independent experiments. (F) hCD4$^+$ Th22 cells were sorted, 10,000 cells were plated in triplicate and then re-stimulated with PMA/Ion. (G) After 4 hrs, Th22 cells were stained with TCRβ, mCD4, hCD4, and Live/Dead dye and analyzed for gMFI of hCD4 by flow cytometry. Error bars represent mean ± SEM. Student's t-test; ***p <0.0001 comparing *Il22*$^{hCD4/null}$ and *Il22*$^{hCD4/hCD4}$. (H) To confirm correlation between hCD4 MFI and IL-22 production, supernatant from sorted and re-stimulated Th22 cells was collected 24 hrs later and analyzed for IL-22 levels by ELISA. Error bars represent mean ± SEM. Student t-test; **p <0.001 comparing *Il22*$^{hCD4/ null}$ and *Il22*$^{hCD4/hCD4}$. (I-J) IELs and LPLs from small intestine, cecum and colon of D9 *C.r*-infected *Rorc*^{EGFP} *Il22*^{hCD4} mice were stimulated with rmIL-23 for 4 hrs and then stained for hCD4, IL-7R, IL-33R, and Live/Dead dye and analyzed by flow cytometry with total cells (I) gated on live IL-7R$^+$ IL-33R$^-$ cells and (J) gated on live IL-7R$^+$ IL-33R$^-$ RORγ$^+$ cells. Numbers in (J) represent percentages of hCD4 (IL-22$^+$) innate cells (TCRβ$^-$) or T cells (TCRβ$^+$). (K) IELs and LPLs from small intestine, cecum and colon of D9 *C.r*-infected *Rorc*^{EGFP}*Il22*^{hCD4} mice were stimulated with rmIL-23 for 4 hrs and then stained with for hCD4, IL-7R, IL-33R, NKp46 and L/D dye and analyzed by flow cytometry (gated on live IL-7R$^+$ IL-33R$^-$ cells). Numbers represent percentages of hCD4 (IL-22$^+$) NK cells (NKp46$^+$). Data shown are concatenated plots from 3 mice. 3-4 mice per time point, 3 independent experiments.

A

	Naive	Day 1	Day 2	Day 3
Ileum	0	0	0	0
Cecum	0	6	19	37
Proximal Colon	0	0.2	0.1	0.1
Middle Colon	0	0.1	0.1	8
Distal Colon	0	0.1	0.1	0.5

TO-PRO-3 / GFP

B

	Naive	Day 3	Day 6	Day 9	Day 13
Cecum	0	26	49	11	3
Colon	0	11	19	19	25

TO-PRO-3 / GFP

C

Cecum: Cr-GFP (log10) vs Naive, D3, D6, D9, D13
*** *** ***

Colon: Cr-GFP (log10) vs Naive, D3, D6, D9, D13
** *** *** ***

D

Il22^hCD4: 37 %, 58 %, 4 %
Il22^Plzf: 14 %, 86 %, 0

hCD4 / TCRβ ; mCd4 / TCRγδ

IL-22+ Colon Cells (#): mCd4+ ILC3 (**), mCd4- ILC3 (*), γδ T cells (*)
□ Il22^hCD4 ■ Il22^Plzf

E

	Cecum	Proximal	Middle	Distal
Il22^hCD4				
Il22^Plzf				

100 μm

Histology Score: Cecum, Prox, Mid, Distal (ns)
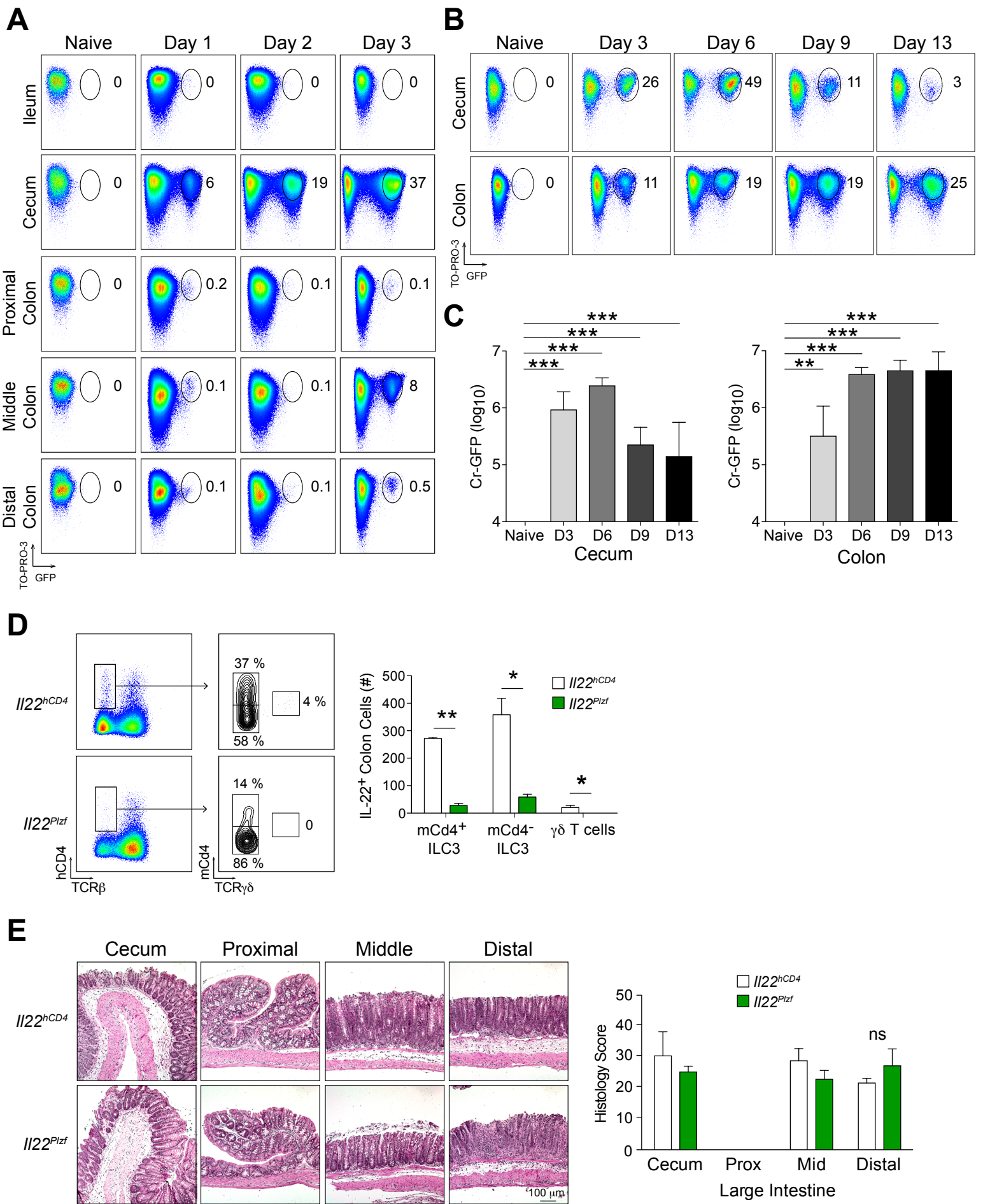□ Il22^hCD4 ■ Il22^Plzf

Large Intestine

Figure S2

Figure S2. Colonization kinetics of *C.r* in the large intestine and Characterization of *Il22*^Plzf^ mice. Related to Figure 2.

(A) *C.r* from supernatants of IEC preps of the distal SI (ileum) and LI (cecum, proximal colon, middle colon, and distal colon) from naïve and D1-D3 *C.r*-GFP-infected BL/6 mice was stained with TO-PRO-3 and analyzed by flow cytometry in log scale. (B) *C.r* from supernatant of IEC preps of cecum and total colon from naïve and *C.r*-infected BL/6 mice at various time points were stained with TO-PRO-3 and analyzed by flow cytometry in log scale. (C) GFP$^+$ TO-PRO-3$^+$ *C.r* was quantitated by flow cytometry using PKH26 reference beads (Sigma). Error bars represent mean $\pm$ SEM. Two-way ANOVA; **p <0.01 and ***p <0.001 comparing naïve and infected. 3 mice per time point, 2 independent experiments. Consistent with pioneering studies (Wiles et al., 2004), *C.r* colonizes the cecum within 24 hrs, followed by colonization in the colon within 3-4 days after inoculation. In addition, *C.r* is cleared from the cecum prior to the colon. Therefore, flow cytometric quantitation allows an accurate assessment of the number of *C.r* attached to epithelial cells from different regions of the colon. (D) Colon LP cells from *C.r*-infected *Il22*^{hCD4} (Control; white) and *Il22*^{Plzf} (Innate-specific IL-22-deletion; green) mice were stimulated with rmIL-23 for 4 hrs and then stained for hCD4, TCRβ, mCD4, TCRγδ and Live/Dead dye and analyzed by flow cytometry. Error bars represent mean $\pm$ SEM. Two-way ANOVA; *p <0.05, **p <0.01 comparing *Il22*^{hCD4} and *Il22*^{Plzf} mice. 2-3 mice per group, 2 independent experiments. (E) LI tissues from d8 *C.r*-infected *Il22*^{hCD4} (white) and *Il22*^{Plzf} (green) mice were stained with hematoxylin and eosin for blinded histology scoring. Scale bar; 100 μm. Error bars represent mean $\pm$ SEM. ns=not significant. 3-5 mice per group, 2 independent experiments.

A

Epithelial Hyperplasia — *Il22^hCD4^* (white), *Il22^EIIa^* (red)
Cecum, Prox, Mid, Distal

Goblet Cell Loss
Cecum *, Prox, Mid, Distal **

Epithelial Degen/Crypt Loss
Cecum **, Prox, Mid, Distal ***

B

Epithelial Hyperplasia — *Il22^hCD4^* (white), *Il22^Plzf^* (green)
Cecum, Prox, Mid, Distal

Goblet Cell Loss — ns
Cecum, Prox, Mid, Distal

Epithelial Degen/Crypt Loss — ns
Cecum, Prox, Mid, Distal

C

*Il22^hCD4^* (white), *Il22^EIIa^* (red)

Liver *
Spleen
CFU/g (log10)
C.r-GFP Day 7

D

*Il22^hCD4^* (white), *Il22^Plzf^* (green)

Liver — ns, Day 6 *
Spleen
CFU/g (log10)
Naive BL/6 (nd), Day 6, Day 9
C.r-GFP

Figure S3

Figure S3. *Il22^{EIIa}* mice have enhanced crypt loss at the peak of *C.r* infection. Related to Figure 3.

(A) LI tissues (cecum, proximal colon, middle colon, and distal colon) from d8 *C.r*-infected *Il22*^hCD4 (Control; white) and *Il22*^EIIa (global IL-22-deficient; red) mice was stained with hematoxylin and eosin for blinded histological scoring of epithelial cell hyperplasia, goblet cell loss and epithelial cell degeneration/crypt loss. (B) LI tissues from d8 *C.r*-infected *Il22*^hCD4 (Control; white) and *Il22*^Plzf (Innate cell-specific IL-22-deficient; green) mice were stained with hematoxylin and eosin for blinded histological scoring of epithelial cell hyperplasia, goblet cell loss and epithelial cell degeneration/crypt loss. (C-D) Log_{10} CFU of *C.r*-GFP in liver and spleen from infected *Il22*^hCD4 (WT) and (C) *Il22*^EIIa or (D) *Il22*^Plzf mice. Error bars represent mean $\pm$ SEM. One-way ANOVA (CFU) and Two-way ANOVA (Histology); *p <0.05, **p <0.01, ***p <0.001 comparing Control and lineage-specific IL-22-deficient mice. ns=not significant. 3-6 mice per group, 2 independent experiments.

A

Middle | Distal

$Il22^{hCD4}$

$Il22^{\Delta Tcell}$

100 μm

□ $Il22^{hCD4}$
■ $Il22^{\Delta Tcell}$

Histology Score

*** ***

Middle | Distal

B

□ $Il22^{hCD4}$
■ $Il22^{\Delta Tcell}$

Epithelial Hyperplasia

ns *** ***

Goblet Cell Loss

*** ***

Epithelial Degen/ Crypt Loss

*

Cecum | Prox | Mid | Distal
Large Intestine

C

□ $Il22^{hCD4}$ ■ $Il22^{\Delta Tcell}$

CFU/g (log10)

* *

Liver | Spleen

D

□ $Il22^{hCD4}$ ■ $Il22^{\Delta Tcell}$

Total IgG (μg/ml)/g feces

**

α-Intimin IgG (μg/ml)/g feces

E

BL/6 | Rag1⁻/⁻

50 μm

C.r-GFP EpCAM1 DAPI

F

Muc1 | Muc2 | UEA1

$Il22^{hCD4}$

$Il22^{\Delta Tcell}$

50 μm | 50 μm | 50 μm

G

Naive | Day 4 | Day 8 | Day 12

91.7 / 4.8 | 89.1 / 6.5 | 76.7 / 18.4 | 34.8 / 59.7

3.3 / 0.1 | 4.3 / 0.1 | 4.8 / 0.1 | 4.6 / 1.0

EpCAM1 / MHCII

MHCII⁺ IECs (%)

***

0 4 8 12
Time (days)

MHCII⁺ IECs (x10³)/ Colon (cm)

**

0 4 8 12
Time (days)

H

$Il22^{hCD4}$ 31.5 %

$Il22^{\Delta Tcell}$ 71.4 %

EpCAM1 / MHC CII

□ $Il22^{hCD4}$ ■ $Il22^{\Delta Tcell}$

MHC CII⁺ IECs/g Colon (x10⁴)

MHC CII⁺ IECs (%)

*

Total IECs/g Colon (x10⁴)

ns

MHC CII on IECs (gMFI)

**

I

$Il22^{hCD4}$ | $Il22^{\Delta Tcell}$

50 μm

CD3 EpCAM1 DAPI

○ $Il22^{hCD4}$ ■ $Il22^{\Delta Tcell}$

CD3⁺ T cells (#) / Crypt length (mm)

***

CD3⁺ T cells (#) / LP (mm²)

ns

Figure S4

Figure S4. *Il22*$^{\Delta \text{Tcell}}$ mice have exacerbated pathology and decreased crypt IEC *Muc1* expression during late phase of *C.r* infection. Related to Figure 4.
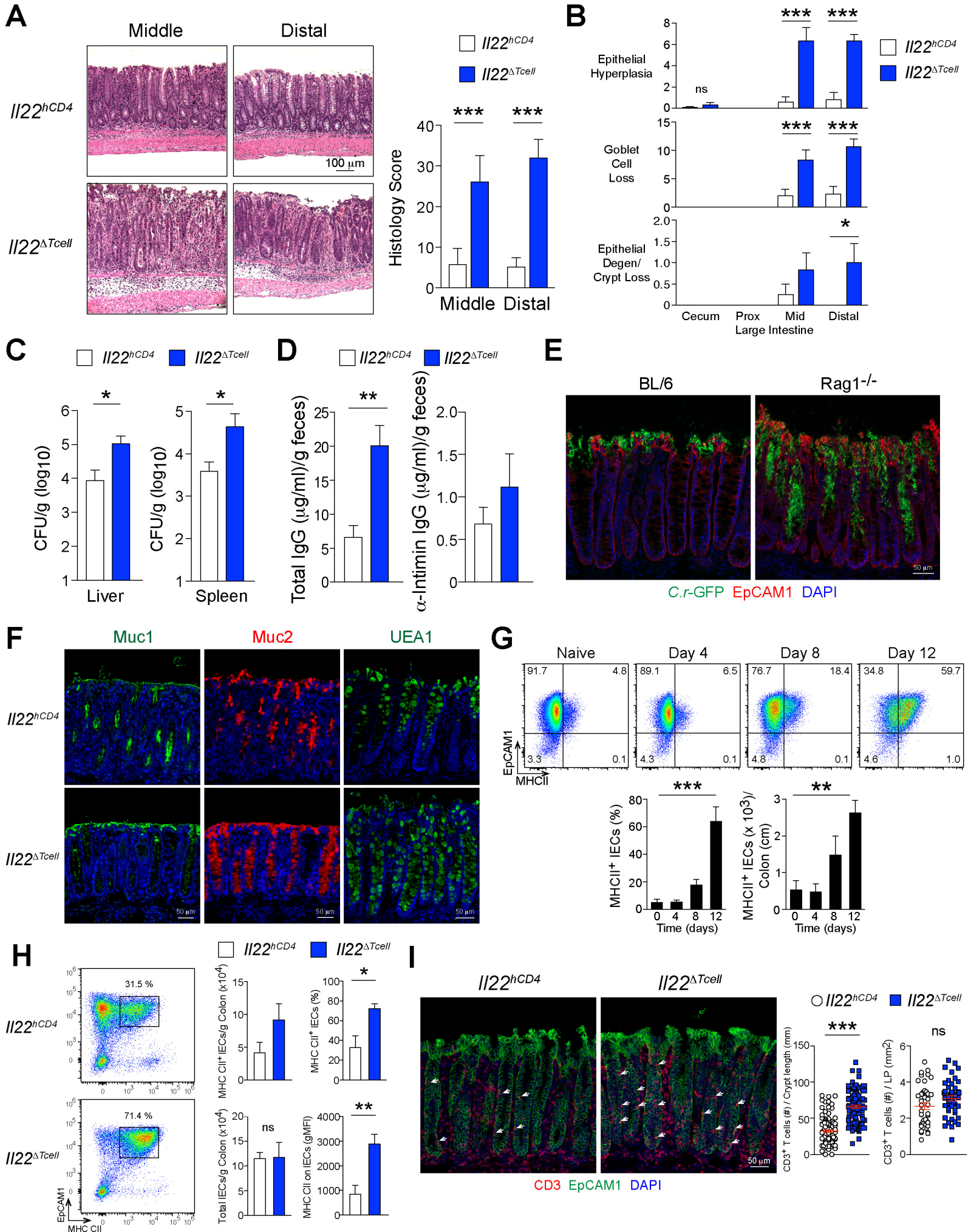
(A-B) LI tissues (cecum, proximal colon, middle colon, and distal colon) from d16 *C.r*-infected *Il22*^{hCD4} (Control; white) and *Il22*$^{\Delta \text{Tcell}}$ (CD4 T cell-specific IL-22-deficient; blue) mice was stained with hematoxylin and eosin for blinded histological scoring of (A) total histology scoring middle and distal colon and (B) epithelial cell hyperplasia, goblet cell loss and epithelial cell degeneration/crypt loss. Scale bar; 100 μm. *Il22*$^{\Delta \text{Tcell}}$ mice have prolonged hyperplasia and crypt loss during the last phase of *C.r* infection when control mice have mostly cleared *C.r* from superficial IECs. Error bars represent mean ± SEM. ns=not significant. Two-way ANOVA; $*p < 0.05$ and $***p < 0.001$ comparing Cntrl and *Il22*$^{\Delta \text{Tcell}}$ mice. 3-5 mice per group, 2 independent experiments. (C) Log$_{10}$ CFU of d9 *C.r*-GFP in liver and spleen from infected *Il22*^{hCD4} (white) and *Il22*$^{\Delta \text{Tcell}}$ (blue) mice. Error bars represent mean ± SEM. One-way ANOVA; $*p < 0.05$ and comparing Cntrl and *Il22*$^{\Delta \text{Tcell}}$ mice. 4-6 mice per group, 2 independent experiments. (D) Supernatant from d13 fecal extracts was analyzed for total IgG and anti-Intimin IgG levels by ELISA. Error bars represent mean ± SEM. Student's t-test; $**p < 0.01$ comparing *Il22*^{hCD4} and *Il22*$^{\Delta \text{Tcell}}$ mice. 3-4 mice per group, 2 independent experiments. Consistent with elevated serum IgG levels in *Il22ra1*$^{-/-}$ mice (Pham et al., 2014), fecal IgG levels were elevated in *Il22*$^{\Delta \text{Tcell}}$ mice compared to controls indicating that IL-22$^+$ T cell-driven crypt protection may not depend on antibody-mediated bacterial clearance. (E) Colon tissue from d13 *C.r*-GFP-infected BL/6 and Rag1$^{-/-}$ mice was stained with GFP, EpCAM1 and DAPI. Scale bar; 50 μm. 4-5 mice per group, 2 independent experiments. (F) Colon tissue from *C.r* D12 *Il22*^{hCD4} and *Il22*$^{\Delta \text{Tcell}}$ mice was stained for Mucin1 (Muc1; green), Mucin2 (Muc2; red) or Ulex Europaeus Agglutinin I Lectin (UEA1; green) and DAPI (blue). Scale bar; 50 μm. 3-4 mice per group, 2 independent experiments. In accord with previous studies (Bergstrom et al., 2008; Lindén et al., 2008), *C.r*-infected control mice exhibited increased Muc1$^+$ and decreased Muc2$^+$ expression on crypt IECs. Since Muc1 and Muc2 play protective roles in bacterial clearance in the intestines (Bergstrom et al., 2010; Lindén et al., 2009), T cell-derived IL-22-driven upregulation of Muc1 on the apical surface of colonic goblet cells likely plays a crucial role in crypt defense by hindering bacterial growth within the crypts during *C.r* infection. (G) Mid/distal colon epithelial cells from naïve and *C.r*-infected BL/6 mice were stained for EpCAM1, MHC CII, CD45 and Live/Dead dye and analyzed by flow cytometry. Error bars represent mean ± SEM. One-way ANOVA; $**p < 0.01$ and $***p < 0.001$ comparing naïve and infected groups. 4 mice per group, 2 independent experiments. MHC CII has been shown to be expressed by colonic IECs in a murine adoptive T cell transfer colitis model (Thelemann et al., 2014). At steady state, surface IECs isolated from colons of naïve mice express *H2-Ab1* mRNA (**Figure 6E**) with approximately 5% of IECs expressing MHC CII protein. Interestingly, as the T cell response increases around day 8-9 after *C.r* inoculation, *H2-Ab1* mRNA is upregulated on SC and LC IECs (**Figure 6E**) with 20% of colonic IECs expressing MHC CII protein. Strikingly, on day 12 when IFNγ responses are heightened, up to 60% of all colonic IECs express MHC CII. (H) Colon cells from IEC prep from d9 *C.r*-infected *Il22*^{hCD4} and *Il22*$^{\Delta \text{Tcell}}$ mice were stained with EpCAM1, MHC CII and Live/Dead dye and analyzed by flow cytometry. Error bars represent mean ± SEM. Student's t-test; $*p < 0.05$ and $**p < 0.01$ comparing d9 *C.r*-infected *Il22*^{hCD4} and *Il22*$^{\Delta \text{Tcell}}$ mice. 4 mice per group, 2 independent experiments. These data support our findings that T cell-derived IL-22 restricts

IFNγ/STAT1 signaling on IECs during *C.r* infection. (I) Colon tissue from d13 *C.r*-infected *Il22^{hCD4}* and *Il22^{ΔTcell}* mice was stained with CD3, EpCAM1 and DAPI. 3 mice per group; ≥30 images pooled per group. Scale bar; 50 μm. Error bars represent mean ± SEM. ns=not significant. Student's t-test; ***p* <0.001 comparing C.r-infected control and *Il22^{ΔTcell}* mice. *Il22^{ΔTcell}* mice have increased numbers of CD3⁺ T cells interacting with crypt IECs with no significant change in T cells in the LP compared to infected control mice. This enhanced T cell-IEC interaction may be the result of elevated MHC CII on IECs or perhaps due to the enhanced expression of the IEC-derived T cell-recruiting chemokine *Cxcl9* (**Figures 6D** and **6E**). Together, these data suggest that upregulation of IFNγ-induced genes on colonic IECs may contribute to recruitment of and antigen presentation to CD4 T cells; however, in the absence of IL-22–producing T cells, IFNγ signaling in IECs is uncontrolled and alone is not sufficient to protection the crypts from bacterial invasion.
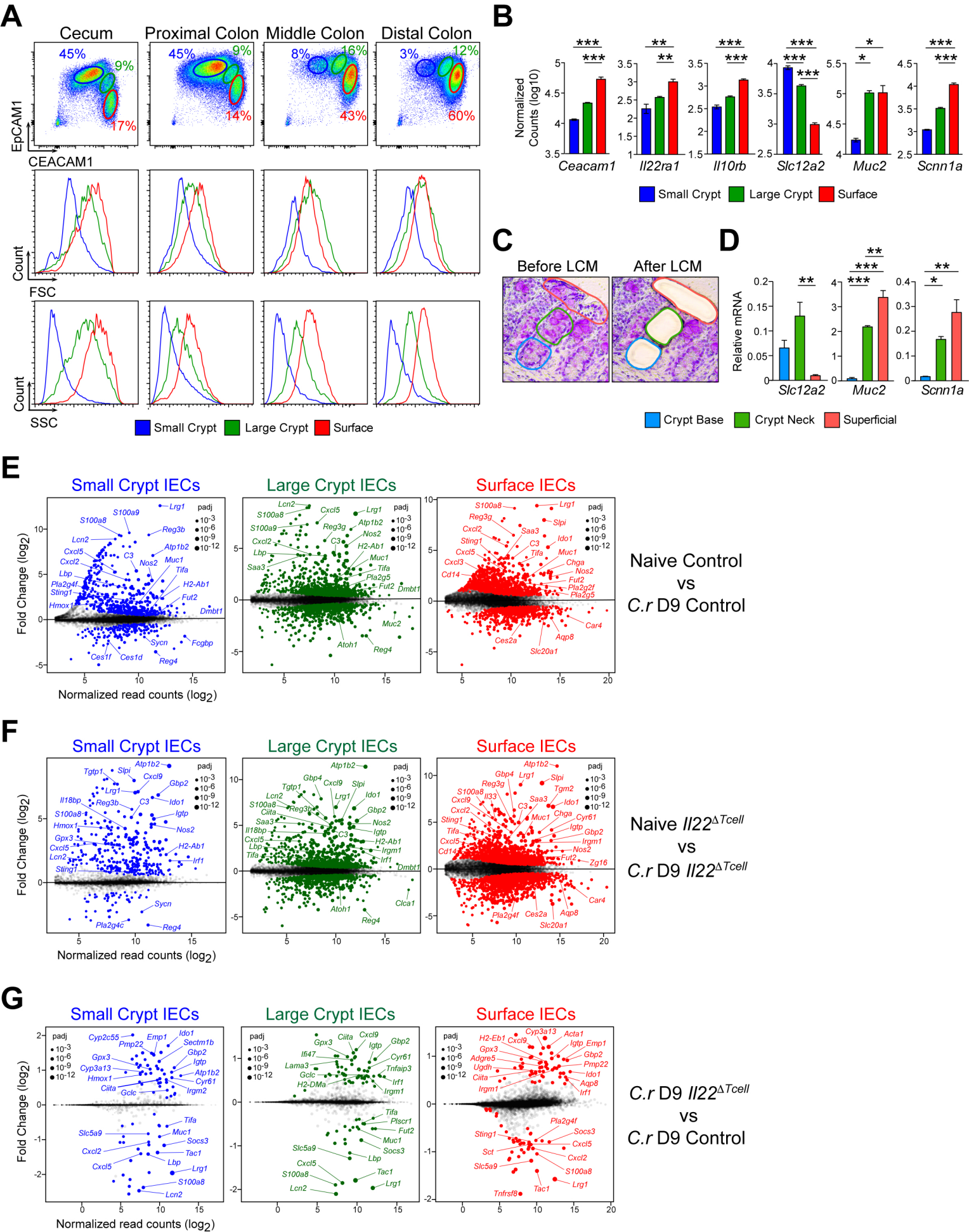
Figure S5

Figure S5. IL-22⁺ T cells amplify genes involved in host defense and reduce genes induced by IFNγ. Related to Figure 6.

(A) Cells from LI tissues (cecum, proximal colon, middle colon and distal colon) were stained for EpCAM1, CEACAM1, CD45 and Live/Dead (L/D) dye and analyzed by flow cytometry. (B) RNA-seq was performed on sorted small crypt (SC) (EpCAM1$^+$ CEACAM1^{lo} FSC^{lo} SSC^{lo} CD45$^-$ L/D dye$^-$; blue), large crypt (LC) (EpCAM1$^+$ CEACAM1^{int} FSC^{int} SSC^{int} CD45$^-$ L/D dye$^-$; green) and surface IECs (Srf) (EpCAM1$^+$ CEACAM1^{hi} FSC^{hi} SSC^{hi} CD45$^-$ L/D dye$^-$; red) from mid/distal colon to determine relative expression of *Ceacam1*, *Il22ra1*, *Il10rb* (pairs with *Il22ra1* to form IL-22R signaling complex), *Slc12a2* (sodium/potassium/chloride transporter expressed by crypt cells (Peña-Münzenmayer et al., 2005), *Muc2* (mucin gene expressed by goblet cells (Allen et al., 1998) and *Scnn1a* (sodium channel expressed by luminal surface IECs (Duc et al., 1994) from naïve BL/6 mice. Counts were normalized by library size. Error bars represent mean $\pm$ SEM. *$p$adj <0.1, **$p$adj <0.01, ***$p$adj <0.001 comparing gene expression between IEC subsets. 2-3 mice per sample, 1-2 independent experiments per naïve group and 3-4 independent experiments per infected group. (C) Colon tissue from naïve BL/6 mice was stained with Cresyl Violet dye and 3 regions of the colon: crypt base (blue), crypt neck (green) and superficial (red) were isolated using laser capture microdissection (LCM). (D) RNA from laser-captured regions of colon tissue were extracted and analyzed by RT-PCR for *Slc12a2*, *Muc2* and *Scnn1a*. Relative mRNA levels were normalized to *Gapdh* and the numbers indicate the quotient of specific gene per *Villin* control mRNA levels. Error bars represent mean $\pm$ SEM. One-way ANOVA; *p <0.05, **p <0.01, ***p <0.001 comparing gene expression between different epithelial regions. Data are representative of 3-4 independent experiments. As expected, *Ceacam1* and *Scnn1a* mRNA expression is higher on Srf IECs compared to crypt IECs. In contrast, the crypt cell marker *Slc12a2* is higher on crypt IECs compared to surface IECs. In addition, Muc2$^+$ cells are found in both the LC and Srf IECs suggesting that goblet cell subsets may have varying levels of *Ceacam1* expression dependent upon their stage of maturation. Interestingly, *Il22ra1* and *Il10rb* mRNA levels are 2-5 fold higher in the Srf IECs compared to crypt IECs indicating that IL-22R expression is highest on mature IECs in the colon. (E-G) MA plots of fold change (log$_2$) versus normalized read counts (log$_2$) show DEGs from SC, LC and Srf IECs from (E) naïve Cntrl versus *C.r* D9 Cntrl, (F) naïve *Il22*$^{\Delta Tcell}$ versus *C.r* D9 *Il22*$^{\Delta Tcell}$ and (G) *C.r* D9 Cntrl versus *C.r* D9 *Il22*$^{\Delta Tcell}$ mice. 2-3 mice per sample, 1-2 independent experiments per naïve group and 3-4 independent experiments per infected group. Several IL-22-inducible genes (e.g., *S100a8*, *Cxcl5*, *Lrg1*, *Tac1*) are upregulated in all IECs from *C.r* D9 Cntrl compared to naïve mice and significantly reduced in infected *Il22*$^{\Delta Tcell}$ compared to infected controls. Furthermore, *Lbp*, *Lcn2* and *Tifa* are significant DEGs in crypt cells only (SC and LC) suggesting that these genes may play an important role in IL-22-mediated T cell-driven crypt protection. In contrast, infected *Il22*$^{\Delta Tcell}$ mice displayed enhanced expression of several IFNγ-inducible genes (e.g., *Gbp2*, *Igtp*, *Cxcl9*) in all IECs compared to infected controls indicating that IL-22/IL-22R/Stat3 signals act to dampen Stat1-driven pro-inflammatory responses in colonic IECs during *C.r* infection.
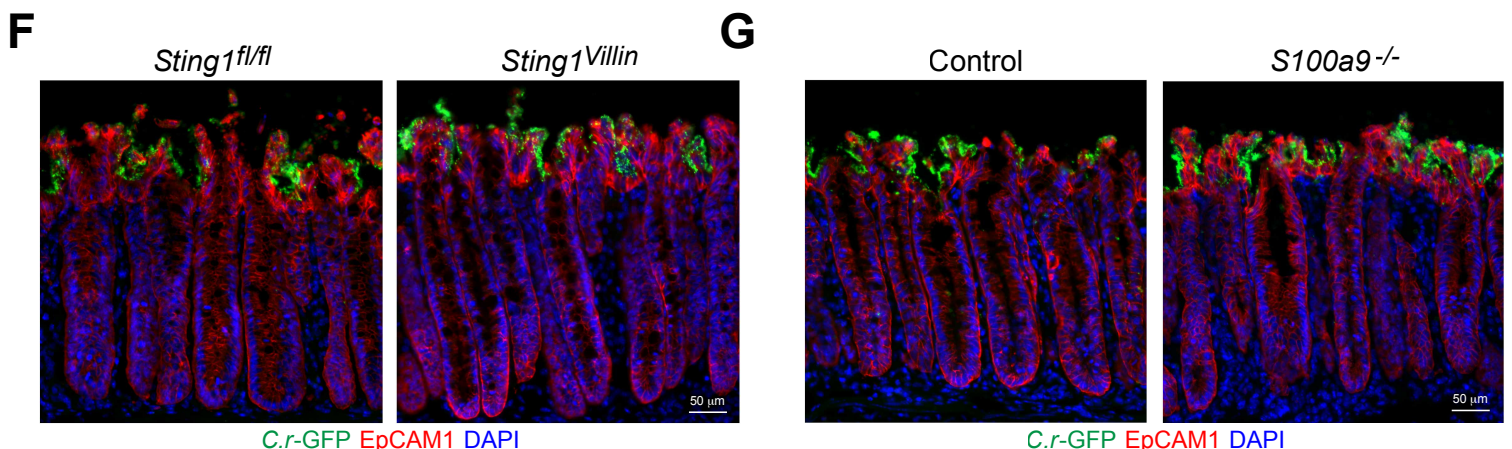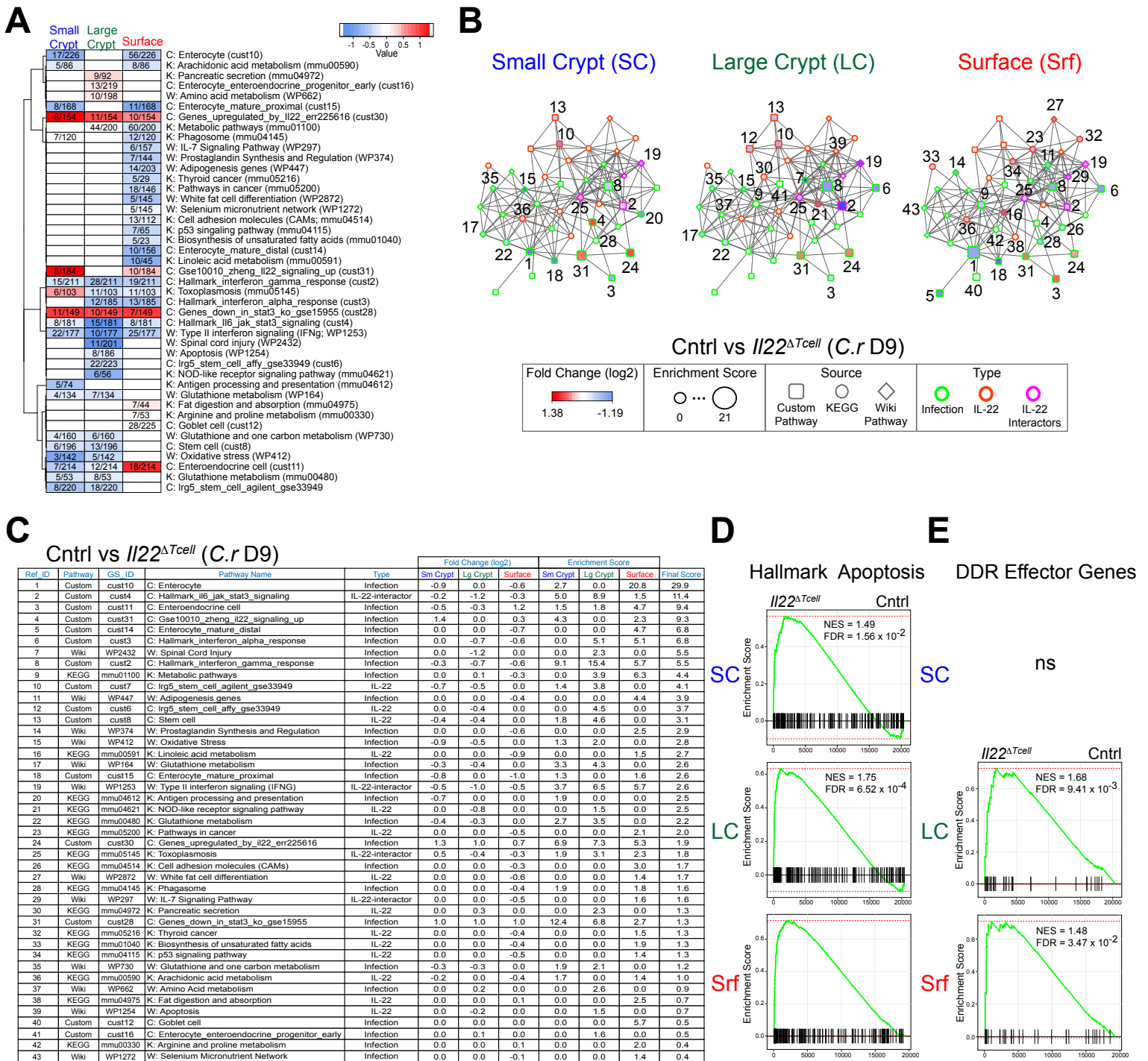
Figure S6

A

Columns: Small Crypt (blue) | Large Crypt (green) | Surface (red)

Small Crypt	Large Crypt	Surface	Pathway
17/226		56/226	C: Enterocyte (cust10)
5/86		8/86	K: Arachidonic acid metabolism (mmu00590)
	9/92		K: Pancreatic secretion (mmu04972)
	13/219		C: Enterocyte_enteroendocrine_progenitor_early (cust16)
	10/198		W: Amino acid metabolism (WP662)
8/168		11/168	C: Enterocyte_mature_proximal (cust15)
8/154	11/154	10/154	C: Genes_upregulated_by_Il22_err225616 (cust30)
	44/200	60/200	K: Metabolic pathways (mmu01100)
7/120		12/120	K: Phagosome (mmu04145)
	6/157		W: IL-7 Signaling Pathway (WP297)
	7/144		W: Prostaglandin Synthesis and Regulation (WP374)
	14/203		W: Adipogenesis genes (WP447)
	5/29		K: Thyroid cancer (mmu05216)
	18/146		K: Pathways in cancer (mmu05200)
	5/145		W: White fat cell differentiation (WP2872)
	5/145		W: Selenium micronutrient network (WP1272)
	13/112		K: Cell adhesion molecules (CAMs; mmu04514)
	7/65		K: p53 signaling pathway (mmu04115)
	5/23		K: Biosynthesis of unsaturated fatty acids (mmu01040)
	10/156		C: Enterocyte_mature_distal (cust14)
	10/45		K: Linoleic acid metabolism (mmu00591)
8/184		10/184	C: Gse10010_zheng_il22_signaling_up (cust31)
15/211	28/211	19/211	C: Hallmark_interferon_gamma_response (cust2)
6/103	11/103	11/103	K: Toxoplasmosis (mmu05145)
	12/185	13/185	C: Hallmark_interferon_alpha_response (cust3)
11/149	10/149	7/149	C: Genes_down_in_stat3_ko_gse15955 (cust28)
8/181	15/181	8/181	C: Hallmark_il6_jak_stat3_signaling (cust4)
22/177	10/177	25/177	W: Type II interferon signaling (IFNg; WP1253)
	11/201		W: Spinal cord injury (WP2432)
	8/186		W: Apoptosis (WP1254)
	22/223		C: Irg5_stem_cell_affy_gse33949 (cust6)
	6/56		K: NOD-like receptor signaling pathway (mmu04621)
5/74			K: Antigen processing and presentation (mmu04612)
4/134	7/134		W: Glutathione metabolism (WP164)
		7/44	K: Fat digestion and absorption (mmu04975)
		7/53	K: Arginine and proline metabolism (mmu00330)
		28/225	C: Goblet cell (cust12)
4/160	6/160		W: Glutathione and one carbon metabolism (WP730)
6/196	13/196		C: Stem cell (cust8)
3/142	5/142		W: Oxidative stress (WP412)
7/214	12/214	18/214	C: Enteroendocrine cell (cust11)
5/53	8/53		K: Glutathione metabolism (mmu00480)
8/220	18/220		C: Irg5_stem_cell_agilent_gse33949

B

Small Crypt (SC) · Large Crypt (LC) · Surface (Srf)

Cntrl vs $Il22^{\Delta Tcell}$ ($C.r$ D9)

Fold Change (log2): 1.38 … -1.19
Enrichment Score: 0 … 21
Source: Custom Pathway (square), KEGG (circle), Wiki Pathway (diamond)
Type: Infection (green), IL-22 (orange), IL-22 Interactors (magenta)

C

Cntrl vs $Il22^{\Delta Tcell}$ ($C.r$ D9)

Ref_ID	Pathway	GS_ID	Pathway Name	Type	Fold Change (log2) Sm Crypt	Lg Crypt	Surface	Enrichment Score Sm Crypt	Lg Crypt	Surface	Final Score
1	Custom	cust10	C: Enterocyte	Infection	-0.9	0.0	-0.6	2.7	0.0	20.8	29.9
2	Custom	cust4	C: Hallmark_il6_jak_stat3_signaling	IL-22-interactor	-0.2	-1.2	-0.3	5.0	8.9	1.5	11.4
3	Custom	cust11	C: Enteroendocrine cell	Infection	-0.5	-0.3	1.2	1.5	1.8	4.7	9.4
4	Custom	cust31	C: Gse10010_zheng_il22_signaling_up	Infection	1.4	0.0	0.3	4.3	0.0	2.3	9.3
5	Custom	cust14	C: Enterocyte_mature_distal	Infection	0.0	0.0	-0.7	0.0	0.0	4.7	6.8
6	Custom	cust3	C: Hallmark_interferon_alpha_response	Infection	0.0	-0.7	-0.6	0.0	5.1	5.1	6.8
7	Wiki	WP2432	W: Spinal Cord Injury	Infection	0.0	-1.2	0.0	0.0	2.3	0.0	5.5
8	Custom	cust2	C: Hallmark_interferon_gamma_response	Infection	-0.3	-0.7	-0.6	9.1	15.4	5.7	5.5
9	KEGG	mmu01100	K: Metabolic pathways	Infection	0.0	0.1	-0.3	0.0	3.9	6.3	4.4
10	Custom	cust7	C: Irg5_stem_cell_agilent_gse33949	IL-22	-0.7	-0.5	0.0	1.4	3.8	0.0	4.1
11	Wiki	WP447	W: Adipogenesis genes	Infection	0.0	0.0	-0.4	0.0	0.0	4.4	3.9
12	Custom	cust6	C: Irg5_stem_cell_affy_gse33949	IL-22	0.0	-0.4	0.0	0.0	4.5	0.0	3.7
13	Custom	cust8	C: Stem cell	IL-22	-0.4	-0.4	0.0	1.8	4.6	0.0	3.1
14	Wiki	WP374	W: Prostaglandin Synthesis and Regulation	Infection	0.0	0.0	-0.6	0.0	0.0	2.5	2.9
15	Wiki	WP412	W: Oxidative Stress	Infection	-0.9	-0.5	0.0	1.3	2.0	0.0	2.8
16	KEGG	mmu00591	K: Linoleic acid metabolism	IL-22	0.0	0.0	-0.9	0.0	0.0	1.5	2.7
17	Wiki	WP164	W: Glutathione metabolism	Infection	-0.3	-0.4	0.0	3.3	4.3	0.0	2.6
18	Custom	cust15	C: Enterocyte_mature_proximal	Infection	-0.8	0.0	-1.0	1.3	0.0	1.6	2.6
19	Wiki	WP1253	W: Type II interferon signaling (IFNG)	IL-22-interactor	-0.5	-1.0	-0.5	3.7	6.5	5.7	2.6
20	KEGG	mmu04612	K: Antigen processing and presentation	Infection	-0.7	0.0	0.0	1.9	0.0	0.0	2.5
21	KEGG	mmu04621	K: NOD-like receptor signaling pathway	IL-22	0.0	-0.8	0.0	0.0	1.5	0.0	2.5
22	KEGG	mmu00480	K: Glutathione metabolism	Infection	-0.4	-0.3	0.0	2.7	3.5	0.0	2.2
23	KEGG	mmu05200	K: Pathways in cancer	IL-22	0.0	0.0	-0.5	0.0	0.0	2.1	2.0
24	Custom	cust30	C: Genes_upregulated_by_il22_err225616	Infection	1.3	1.0	0.7	6.9	7.3	5.3	1.9
25	KEGG	mmu05145	K: Toxoplasmosis	IL-22-interactor	0.5	-0.4	-0.3	3.1	3.1	2.3	1.8
26	KEGG	mmu04514	K: Cell adhesion molecules (CAMs)	Infection	0.0	0.0	-0.3	0.0	0.0	3.0	1.7
27	Wiki	WP2872	W: White fat cell differentiation	IL-22	0.0	0.0	-0.6	0.0	0.0	1.4	1.7
28	KEGG	mmu04145	K: Phagasome	Infection	0.0	0.0	-0.4	1.9	0.0	1.8	1.6
29	Wiki	WP297	W: IL-7 Signaling Pathway	IL-22-interactor	0.0	0.0	-0.5	0.0	0.0	1.6	1.6
30	KEGG	mmu04972	K: Pancreatic secretion	IL-22	0.0	0.3	0.0	0.0	2.3	0.0	1.3
31	Custom	cust28	C: Genes_down_in_stat3_ko_gse15955	Infection	1.0	1.0	1.0	12.4	6.8	2.7	1.3
32	KEGG	mmu05216	K: Thyroid cancer	IL-22	0.0	0.0	-0.4	0.0	0.0	1.5	1.3
33	KEGG	mmu01040	K: Biosynthesis of unsaturated fatty acids	IL-22	0.0	0.0	0.0	0.0	0.0	1.9	1.3
34	KEGG	mmu04115	K: p53 signaling pathway	IL-22	0.0	0.0	-0.5	0.0	0.0	1.4	1.3
35	Wiki	WP730	W: Glutathione and one carbon metabolism	Infection	-0.3	-0.3	0.0	1.9	2.1	0.0	1.2
36	KEGG	mmu00590	K: Arachidonic acid metabolism	IL-22	-0.2	0.0	-0.4	1.7	0.0	1.4	1.0
37	Wiki	WP662	W: Amino Acid metabolism	Infection	0.0	0.2	0.0	0.0	2.6	0.0	0.9
38	KEGG	mmu04975	K: Fat digestion and absorption	IL-22	0.0	0.0	0.1	0.0	0.0	2.5	0.7
39	Wiki	WP1254	W: Apoptosis	IL-22	0.0	-0.2	0.0	0.0	1.5	0.0	0.7
40	Custom	cust12	C: Goblet cell	Infection	0.0	0.0	0.0	0.0	5.7	0.0	0.5
41	Custom	cust16	C: Enterocyte_enteroendocrine_progenitor_early	Infection	0.0	0.1	0.0	0.0	1.6	0.0	0.5
42	KEGG	mmu00330	K: Arginine and proline metabolism	Infection	0.0	0.0	0.1	0.0	0.0	2.0	0.4
43	Wiki	WP1272	W: Selenium Micronutrient Network	Infection	0.0	0.0	-0.1	0.0	0.0	1.4	0.4

D

Hallmark Apoptosis

$Il22^{\Delta Tcell}$ — Cntrl

SC: NES = 1.49, FDR = 1.56×10^{-2}

LC: NES = 1.75, FDR = 6.52×10^{-4}

Srf: (enrichment plot)

E

DDR Effector Genes

$Il22^{\Delta Tcell}$ — Cntrl

SC: ns

LC: NES = 1.68, FDR = 9.41×10^{-3}

Srf: NES = 1.48, FDR = 3.47×10^{-2}

F

$Sting1^{fl/fl}$ · $Sting1^{Villin}$

$C.r$-GFP EpCAM1 DAPI

Scale bar: 50 µm

G

Control · $S100a9^{-/-}$

$C.r$-GFP EpCAM1 DAPI

Scale bar: 50 µm

Figure S6

Figure S6. Pathway network analysis identifies DEGs mapping to Enterocyte-specific, oxidative stress and metabolic pathway genes. Related to Figure 7.

(A-C) RNA-seq was performed on sorted colon IECs from D9 *C.r*-infected *Il22*[hCD4] (Control) and *Il22*[ΔTcell] (CD4 T cell-specific IL-22-deficient) mice. (A) Heatmap of the average expression of significant DEGs in Wiki (W), KEGG (K) and Custom IEC (C) pathways was generated using Pager 2.0 (Yue et al., 2015, 2017). Color represents DEGs upregulated in *C.r* D9 Cntrl mice (red) and DEGs upregulated in *C.r* D9 *Il22*[ΔTcell] mice (blue). Color gradient represents the average of the DEGs ($\log_2$ fold change). Numbers in the graph represent the DEG hits per size of the pathway. (B) Co-membership network was generated using Pager 2.0 (Yue et al., 2015, 2017) to display the comparison between DE pathways in small crypt (SC), large crypt (LC) and surface (Srf) IECs from *C.r* D9 Cntrl and *C.r* D9 *Il22*[ΔTcell] mice. Color inside the symbol depicts fold change ($\log_2$, pathway upregulated in Cntrl (red), pathway upregulated in *Il22*[ΔTcell] (blue)), size of the symbol depicts enrichment score, shape of the symbol depicts source (Custom Pathway (square), KEGG (circle), Wiki Pathway (diamond)), and border color depicts type of interaction (Infection (green), IL-22 (orange), IL-22 interactors (pink)). Numbers represent reference identification (Ref ID) of pathways. (C) Table of the Wiki (W), KEG (K) and IEC Custom (C) pathways was generated with the pathways ranked by the final score. The final score is calculated by the sum of the pairwise distance of the sample log2 Fold Change multiplied by the sum of the pairwise distance of the sample Enrichment Score. The original links to the WikiPathways can be retrieved by www.wikipathways.org/index.php/Pathway:[GS_ID], and the original links to the KEGG Pathways can be retrieved by www.genome.jp/kegg-bin/show_pathway?[GS_ID]. (D-E) Bar code plots of GSEA of (D) Hallmark Apoptosis and (E) DNA damage response (DDR) Effector Genes in small crypt (blue), large crypt (green) and surface (red) IECs from *C.r* D9 Cntrl mice versus *C.r* D9 *Il22*[ΔTcell] mice. NES, normal enrichment score; FDR, false discovery rate. 2-3 mice per sample, 3-4 independent experiments per group. (F, G) Colon tissue from *C.r*-GFP-infected (F) *Sting1*^{fl/fl} and *Sting1*[VIIIin] (*Sting1*^{fl/fl} x *Villin/Cre*) mice, or (G) *C.r*-GFP-infected Control and *S100a9*^{−/−} mice was stained for GFP (green), EpCAM1 (red) and DAPI (blue). Scale bar, 50 μm. 4-5 mice per group, 2 independent experiments. These data indicate that deficiency in either *Sting1* or *S100a9* alone is dispensable for crypt protection during *C.r* infection. As expected, DEGs in IL-22/Stat3 pathways (cust4, cust28, cust30, cust31) are heightened in all IEC subsets (small crypt, large crypt, surface) from *C.r* D9 Cntrl mice compared to *C.r* D9 *Il22*[ΔTcell] mice. In addition, DEGs associated with pancreatic secretion (mmu04972), and fat digestion and absorption (mmu04975) (e.g., *Pla2g2a, Pla2g2f* and *Pla2g5*) are enriched in large crypt and surface IECs. DEGs associated with amino acid metabolism (e.g., *Gsr, Mdh2, Tat*) are also enriched in LC IECs from *C.r* D9 Cntrl mice. In contrast, DEGs in IFNα and IFNγ pathways (cust2, cust3, WP1253) are increased in *C.r* D9 *Il22*[ΔTcell] mice compared to controls. Moreover, in the absence of T cell-derived IL-22, DEGs associated with glutathione metabolism and oxidative stress (e.g., *Gpx3, Gclc, Hmox1*) are heightened in small crypt and large crypt IECs. Consistent with these findings, DEGs involved in apoptosis and the DDR pathway are also elevated in *C.r*-infected *Il22*[ΔTcell] mice compared to controls. Taken together, this is likely due to bacterial overgrowth in the crypts and consequently may contribute to the enhanced pathology observed in colons of *Il22*[ΔTcell] mice (**Figures S4A** and **S4B**).